 736

CONFIDENTIAL

NASA TM X-300

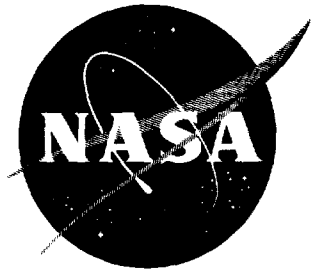

TECHNICAL MEMORANDUM

X-300

AN ANALYTICAL INVESTIGATION OF ABLATION

By Bernard Rashis and Russell N. Hopko

Langley Research Center
Langley Field, Va.

NATIONAL AERONAUTICS AND SPACE ADMINISTRATION

WASHINGTON

July 1960

CONFIDENTIAL

CONFIDENTIAL

NATIONAL AERONAUTICS AND SPACE ADMINISTRATION

TECHNICAL MEMORANDUM X-300

AN ANALYTICAL INVESTIGATION OF ABLATION*

By Bernard Rasnis and Russell N. Hopko

SUMMARY

An analytical procedure is described which enables the derivation of effective heat of ablation relationships for any type of boundary layer from transpiration cooling results. The procedure enables the inclusion of such effects as the ratio of wall temperature to local stream temperature, surface radiation, and surface combustion.

The predicted effective heats of ablation for a three-dimensional laminar stagnation boundary layer for Teflon material were in agreement with those derived from tests conducted at boundary-layer enthalpy potentials of 800 and approximately 7,000 Btu/lb.

The predicted equilibrium surface temperatures on nonablating surfaces behind an ablating material were in agreement with the values derived from tests conducted with Inconel cylinders having Teflon hemispherical nose pieces.

INTRODUCTION

Previous experimental investigations (refs. 1, 2, and 3) have indicated that ablating materials have considerable promise as a cooling or heat-blocking system for high-speed vehicles, from a standpoint of simplicity as well as efficiency. Reference 4 gives the framework of an excellent theoretical treatment which shows how the similarity parameters of ablation are related to the parameters of transpiration cooling. The analysis of reference 4 does not, however, include the effects of different values of the ratio of wall temperature to local stream temperature nor does it include ablating materials having specific heat values different from those of air.

The purpose of this paper is to show how expressions relating the ablation parameters to the material and boundary-layer characteristics may be derived for any type of boundary layer, simply and directly from transpiration cooling results.

*Title, Unclassified.

SYMBOLS

C	velocity gradient
c_p	specific heat, Btu/lb-$^{\circ}$F
F	ratio of coolant mass-flow rate to local air mass-flow rate
f	fraction of vaporization
G	average value of coolant flow rate, lb/(sq ft)(sec) over injection area
H	enthalpy, Btu/lb
h	heat-transfer coefficient, Btu/(sq ft)(sec)($^{\circ}$F)
h_{eff}	effective heat of ablation, Btu/lb

$$h_{ov} = f\left[L_{vap} + \frac{1}{3}c_{p,melt}\left(T_{vap} - T_{melt}\right)\right] + \left[\frac{2}{3}c_{p,melt}\left(T_{vap} - T_{melt}\right) + L_{melt} + c_{p,solid}\left(T_{melt} - T_{solid}\right)\right]$$

L	latent heat, Btu/lb
M	molecular weight
$\dot{m}$	mass ejection rate, lb/(sq ft)(sec)
N_{Nu}	Nusselt number
N_{Pr}	Prandtl number
N_{Re}	Reynolds number
N_{St}	Stanton number
q	heat flux, Btu/(sq ft)(sec)
q_{ϕ}	heat transfer from gas layer to ablating surface (see eq. (1))

S	surface area, sq ft
T	temperature, ^{o}F
t	wall thickness, ft
V	velocity, ft/sec
W	mass fraction of foreign gas
w	mass flow, lb/sec
x	porous length plus downstream length, ft
x_o	porous length, ft
Δ	heat of combustion, Btu/lb
ϵ	emissivity
η	boundary-layer recovery factor

$$\eta_{comb} = \frac{\Delta q_{comb}}{q_{aero}}$$

$$\eta_{rad} = \frac{\Delta q_{rad}}{q_{aero}}$$

ν	kinematic viscosity, ft^2/sec
ρ	density, lb/cu ft
σ	Boltzman's constant
τ	time

Subscripts:

aero	aerodynamic
air	air
aw	adiabatic wall
c	coolant

comb	combustion
e	equilibrium
gas	gas
l	local
le	portion of leading-edge area that is supplying coolant
m	mixture
melt	liquid film or melting
o	zero coolant flow or no ablation
p	porous area
rad	radiation
solid	solid material
sub	sublimation
t	total
vap	vaporized layer or vaporization
w	wall
w,air	air at wall temperature
ξ	downstream of porous area
∞	free stream

ANALYSIS

In figure 1(a), there is shown a schematic diagram of a body undergoing ablation at the stagnation point. The body is heated and melts, the melt forming a liquid film. This film or a portion thereof is then vaporized, the vaporized material forming a gas layer. This process is hereinafter referred to as ablation by melting and vaporization. In figure 1(b), typical temperature variations are shown for the different phases.

Defining q_ϕ as the heat transfer from the gas layer to the ablating surface, the general heat-balance equation for the body of figure 1 can be written (ref. 5) as

$$q_\phi = \dot{m}_{vap}\left[L_{vap} + \tfrac{1}{3}c_{p,melt}\left(T_{vap} - T_{melt}\right)\right] + \dot{m}_{melt}\left[\tfrac{2}{3}c_{p,melt}\left(T_{vap} - T_{melt}\right) + L_{melt} + c_{p,solid}\left(T_{melt} - T_{solid}\right)\right] \quad (1)$$

where $\dot{m}_{melt}$ is the amount of material melted per second and $\dot{m}_{vap}$ is the amount vaporized per second.

If the heat transfer to a nonablating surface which is at the same temperature as the ablating surface is denoted by q_{aero}, equation (1) can be written as

$$\frac{q_\phi}{q_{aero}} = \frac{\left\{\dot{m}_{vap}\left[L_{vap} + \tfrac{1}{3}c_{p,melt}\left(T_{vap} - T_{melt}\right)\right] + \dot{m}_{melt}\left[\tfrac{2}{3}c_{p,melt}\left(T_{vap} - T_{melt}\right) + L_{melt} + c_{p,solid}\left(T_{melt} - T_{solid}\right)\right]\right\}}{q_{aero}} \quad (2)$$

For a melting-vaporizing system if f is defined as that fraction of the melt which is vaporized, or

$$\dot{m}_{vap} = f\dot{m}_{melt}$$

equation (2) becomes

$$\frac{q_\phi}{q_{aero}} = \dot{m}_{melt}\frac{\left\{f\left[L_{vap} + \tfrac{1}{3}c_{p,melt}\left(T_{vap} - T_{melt}\right)\right] + \left[\tfrac{2}{3}c_{p,melt}\left(T_{vap} - T_{melt}\right) + L_{melt} + c_{p,solid}\left(T_{melt} - T_{solid}\right)\right]\right\}}{q_{aero}} \quad (3)$$

If the term that is multiplied by $\dot{m}_{melt}$ is denoted by h_{ov} and an effective heat absorption parameter that takes into account both the heat absorbed by the ablating material and the heat shielding effect of its vapor is defined as

$$h_{eff} = \frac{q_{aero}}{\dot{m}_{melt}}$$

CONFIDENTIAL

there results

$$\frac{q_\phi}{q_{aero}} = \frac{\dot{m}_{melt} h_{ov}}{q_{aero}} = \frac{h_{ov}}{h_{eff}}$$

Since the term $\frac{q_\phi}{q_{aero}}$ is analogous to the shielding-effect ratio $\frac{N_{St}}{N_{St,aero}}$ obtained from transpiration cooling, then

$$\frac{N_{St}}{N_{St,aero}} = \frac{h_{ov}}{h_{eff}} \tag{4}$$

The transpiration cooling flow rate correlation parameter defined as

$$\frac{F}{N_{St,aero}} \frac{c_{p,c}}{c_{p,l}} = \frac{\frac{\dot{m}_{vap}}{(\rho V)_l}}{\frac{q_{aero}}{(\rho V)_l c_{p,l} (T_{aw} - T_w)}} \frac{c_{p,c}}{c_{p,l}}$$

can be written as

$$\frac{F}{N_{St,aero}} \frac{c_{p,c}}{c_{p,l}} = \frac{\dot{m}_{vap}}{q_{aero}} (H_{aw} - H_{w,air}) \frac{c_{p,c}}{c_{p,l}}$$

$$= \frac{\dot{m}_{melt} f (H_{aw} - H_{w,air})}{q_{aero}} \frac{c_{p,c}}{c_{p,l}}$$

$$= \frac{f (H_{aw} - H_{w,air})}{h_{eff}} \frac{c_{p,c}}{c_{p,l}}$$

but from equation (4)

$$h_{eff} = h_{ov} \frac{N_{St,aero}}{N_{St}}$$

Thus,

$$\frac{F}{N_{St,aero}} \frac{c_{p,c}}{c_{p,l}} = \frac{f\left(H_{aw} - H_{w,air}\right)}{h_{ov}} \frac{N_{St}}{N_{St,aero}} \frac{c_{p,c}}{c_{p,l}}$$

and

$$\frac{\frac{F}{N_{St,aero}} \frac{c_{p,c}}{c_{p,l}}}{\frac{N_{St}}{N_{St,aero}}} = \frac{f\left(H_{aw} - H_{w,air}\right)}{h_{ov}} \frac{c_{p,c}}{c_{p,l}} \tag{5}$$

Hence, once the relationship between $N_{St}/N_{St,aero}$ and $\left(F/N_{St,aero}\right)\left(c_{p,c}/c_{p,l}\right)$ is known from transpiration data, the transformation relationships (eqs. (4) and (5)) enable the solution of h_{eff} in terms of the enthalpy difference $H_{aw} - H_{w,air}$ and the intrinsic heat capacity of the material h_{ov}. Thus, once the shielding relationship is known for any boundary-layer type and vapor, evaluation of the material overall effectiveness depends only on the material properties in the solid and molten states, and the quantity f.

A discussion of f (percent of vaporization) is given in reference 6. Briefly, f increases with flight speed at constant pressure and decreases with increase in pressure at constant flight speed. For any given flight conditions, f increases with the Prandtl number of the melt.

For the case where radiation, combustion, and other effects modify the reference heat-transfer rate, an actual effective heat of ablation parameter is defined as

$$h_{eff}^{*} = \frac{h_{eff}}{1 + \eta_1 + \eta_2 + \ldots \eta_n}$$

where

$$\eta = \pm \frac{\Delta q}{q_{aero}}$$

the plus or minus sign depending on whether Δq adds or subtracts heat from q_{aero}.

For example, the effect of radiation from the surface is to decrease the reference heat-transfer rate; thus,

$$1 - \eta_{rad} = 1 - \frac{\Delta q_{rad}}{q_{aero}} = 1 - \frac{0.48\left[\epsilon^{1/4}\left(\frac{T_w}{1000}\right)\right]^4}{q_{aero}}$$

and is equal to 1 when Δq_{rad} is zero $\left(\epsilon^{1/4}T_w = 0\right)$ and is equal to zero when the numerical value of the parameter $\epsilon^{1/4}T_w$ is equal to the radiation equilibrium temperature. Some representative values of $1 - \eta_{rad}$ are shown in figure 2.

The actual mass losses $\dot{m}^*$ are thus defined as

$$\dot{m}^* = \frac{q_{aero}}{h_{eff}^*}$$

and the ratio

$$\frac{\dot{m}^*}{\dot{m}} = \frac{h_{eff}}{h_{eff}^*}$$

The effect of combustion would be to increase the reference heat-transfer rate; thus,

$$1 + \eta_{comb} = 1 + \frac{\Delta q_{comb}}{q_{aero}}$$

The following expression has been derived in reference 7:

$$\frac{q_\phi'}{q_\phi} = \frac{H_{aw} - H_{w,air} + KW_\infty \Delta}{H_{aw} - H_{w,air}} \tag{6}$$

where

q_ϕ' heat transfer from gas layer to ablating surface when combustion occurs

K ratio of molecular weight of product to that of oxidizer

W_∞ mass fraction of oxidizer evaluated at outer edge of boundary layer

Δ heat of combustion per pound of product

The above expression is valid only for laminar boundary layers and assumes a Lewis number of 1.0 (Prandtl number = Schmidt number). It applies to the cases where the mass flow of oxygen to the surface is a maximum. This maximum flow rate of oxygen is assumed to be completely consumed in the reaction. Below some small value of the mass-flow rate of the combustible coolant corresponding to stoichiometric surface combustion, the expression is no longer valid.

Upon rearrangement, equation (6) can be written as

$$\frac{q_\phi' - q_\phi}{q_{aero}} = \frac{\Delta q_{comb}}{q_{aero}} = \frac{h_{ov}}{h_{eff}} \frac{KW_\infty\left(\frac{\Delta}{H_{w,air}}\right)}{\left(\frac{H_{aw} - H_{w,air}}{h_{ov}}\right)\frac{c_{p,c}}{c_{p,l}}}$$

Since

$$\frac{q_\phi}{q_{aero}} = \frac{h_{ov}}{h_{eff}}$$

and

$$H_{w,air} = \frac{c_{p,l}}{c_{p,c}} h_{ov}$$

thus,

$$1 + \eta_{comb} = 1 + \frac{h_{ov}}{h_{eff}} \frac{KW_\infty\left(\frac{\Delta}{H_{w,air}}\right)}{\left(\frac{H_{aw} - H_{w,air}}{h_{ov}}\right)\frac{c_{p,c}}{c_{p,l}}}$$

and is equal to 1.0 for no combustion ($\Delta = 0$) and approaches maximum values for stoichiometric combustion at the surface. Some representative values of $1 + \eta_{comb}$ are shown in figure 3. The curve for $\frac{K\Delta}{H_{w,air}} = 15$ represents the chemical reaction

$$2H_2 + O_2 \xrightarrow{\Delta} 2H_2O$$

The curve for $\frac{K\Delta}{H_{w,air}} = 20$ represents the combustion of Teflon. Reference 6 gives the reactions and Δ values for this material.

Derivation of Shielding-Effect Relationships

In the preceding section, it was shown that effective heat of ablation relationships may be obtained directly from transpiration cooling results. In this section, several available theoretical and experimental transpiration cooling results for several types of boundary-layer flows will be transformed into the pertinent ablation cooling parameters by means of equations (4) and (5).

Two-dimensional turbulent.- Reference 8 gives experimental results for helium-to-air and nitrogen-to-air transpiration cooling of a two-dimensional 20° half-angle wedge for a free-stream Mach number of 2.0 and stagnation temperatures ranging from 1,295° F to 2,910° F. The results of reference 8 are presented in that paper as the shielding-effect ratio $\frac{N_{St}}{N_{St,aero}}$ as a function of the flow-rate parameter $\frac{F}{N_{St,aero}}$. However, it can be shown that to a good approximation (see appendix) the coolant weight requirements, for the same cooling ratio, or

$$\left(\frac{N_{St}}{N_{St,aero}}\right)_{helium\text{-}to\text{-}air} = \left(\frac{N_{St}}{N_{St,aero}}\right)_{air\text{-}to\text{-}air}$$

are inversely proportional to the specific heats of the coolants, or

$$\left(Fc_{p,c}\right)_{helium} = \left(Fc_{p,c}\right)_{air}$$

Thus, the data of reference 8 were modified by multiplying the parameter $\frac{F}{N_{St,aero}}$ by the corresponding ratios of $\frac{c_{p,c}}{c_{p,l}}$ where $c_{p,c}$, the coolant specific heat, was evaluated at the cooled wall temperature, and $c_{p,l}$, the stream specific heat, was evaluated at the local temperature. The modified results are shown in figure 4.

In reference 9, there is derived a simple expression for the shielding effect of transpiration for a two-dimensional turbulent boundary layer. The expression can be written as

$$\frac{N_{St}}{N_{St,aero}} = \frac{\frac{F}{N_{St,aero}} \frac{c_{p,c}}{c_{p,l}}}{\exp\left(\frac{F}{N_{St,aero}} \frac{c_{p,c}}{c_{p,l}}\right) - 1}$$

The curve computed from this expression is also shown in figure 4 (dashed curve). The theoretical values of reference 9 are somewhat higher than the experimental data of reference 8. It should be noted, however, that the theory of reference 9 is for T_w/T_l equal to 1.0, whereas the data of reference 8 were for values of T_w/T_l ranging from approximately 1/8 to slightly less than 1.0. Since the shielding-effect ratio would decrease somewhat for decreasing T_w/T_l, the difference between the two curves of figure 4 is probably due to this effect. Unfortunately, the experimental scatter in the data of reference 8 precludes any delineation of the T_w/T_l effect.

Two-dimensional laminar.- Reference 10 gives theoretical transpiration cooling results for air-to-air and values of T_w/T_l of 1.0, 1/2, and 1/4. The results of reference 10 are presented in terms of a heat-transfer parameter $\frac{N_{Nu,w}}{\sqrt{N_{Re,w}}}$ and a nondimensional flow rate outward from the porous surface f_w. Although reference 10 computes the cases for values of T_w/T_l other than 1.0 by the procedure described it was found that by dividing f_w by the ratio $\left(T_w/T_l\right)^{0.095}$, the values of the ratio

$$\frac{\left(N_{Nu,w}/\sqrt{N_{Re,w}}\right)_{fw\neq 0}}{\left(N_{Nu,w}/\sqrt{N_{Re,w}}\right)_{fw=0}}$$

all fell on a single curve as shown in figure 5.

Since the preceding ratio is analogous to the ratio $\frac{N_{St}}{N_{St,aero}}$ and

$$\left(\frac{F}{N_{St,aero}}\right)_{T_w/T_l=1.0} = \left[\frac{(-f_w)N_{Pr,w}}{2\left(\frac{N_{Nu,w}}{N_{Re,w}}\right)_{f_w=0}}\right]_{T_w/T_l=1.0}$$

the results of reference 9 when plotted as the ratio $\frac{N_{St}}{N_{St,aero}}$ against the ratio

$$\frac{\left(\frac{F}{N_{St,aero}}\right)_{T_w/T_l=1.0}\frac{c_{p,c}}{c_{p,l}}}{\left(T_w/T_l\right)^{0.095}}$$

provides the shielding curve for a two-dimensional laminar boundary layer applicable also to the cases where T_w/T_l is different than 1 and also where the transpired coolant has properties different than air..

Two- and three-dimensional laminar stagnation.- Reference 11 gives theoretical transpiration cooling results for air-to-air and T_w/T_l equal to 1.0, 0.5, and 0.25. The results of reference 11 are given in terms of the heat-transfer parameter $N_{Nu,w}/\sqrt{N_{Re,w}}$ and a nondimensional normal velocity outward from the porous surface $V_w/\sqrt{\nu_w C}$. However, for the two-dimensional stagnation case

$$(-f_w) = \frac{V_w}{\sqrt{\nu_w C}}$$

and for the three-dimensional stagnation case

$$(-f_w) = \frac{\sqrt{3}}{2}\left(\frac{V_w}{\sqrt{\nu_w C}}\right)$$

As shown in figure 6, the results of reference 10 when plotted as the ratio

$$\left(N_{Nu,w}/\sqrt{N_{Re,w}}\right)_{V_w \neq 0} \Big/ \left(N_{Nu,w}/\sqrt{N_{Re,w}}\right)_{V_w = 0}$$

against the ratio

$$\frac{V_w/\sqrt{\nu_w C}}{\left(T_w/T_l\right)^{0.19}}$$

reproduce as single curves. Since

$$\left(\frac{F}{N_{St,aero}}\right)_{T_w/T_l=1.0} = \left[\frac{\left(\frac{V_w}{\sqrt{\nu_w C}}\right)N_{Pr,w}}{\left(\frac{N_{Nu,w}}{\sqrt{N_{Re,w}}}\right)_o}\right]_{T_w/T_l=1.0}$$

the results of reference 10 when the ratio $\frac{N_{St}}{N_{St,aero}}$ is plotted as a function of the ratio

$$\frac{\left(\frac{F}{N_{St,aero}}\right)_{T_w/T_l=1.0} \frac{c_{p,c}}{c_{p,l}}}{\left(T_w/T_l\right)^{0.19}}$$

provide the shielding curves for the two- and three-dimensional laminar stagnation boundary-layer cases, applicable to all coolants and values of T_w/T_l. Use of the transformation equations (4) and (5) converts the shielding curves into the curves applicable to ablating materials.

Figure 7 shows the effective heat of ablation curves that were obtained from the shielding curves previously discussed for the case where T_w/T_l is 1.

Comparison of Experiment and Theory

Figure 8 shows h_{eff} of Teflon as a function of the ratio

$$\frac{\left(H_{aw} - H_{w,air}\right)}{\left(T_w/T_l\right)^{0.19}} \frac{c_{p,c}}{c_{p,l}}$$

for three-dimensional laminar stagnation flow. The circular symbols denote the experimental values derived in reference 3. The enthalpy potential ratio was evaluated using a value of 900 Btu/lb for h_{ov}. The values of T_w and $c_{p,c}$ were obtained from figures 9 and 10, respectively. The curves of figures 9 and 10 were obtained from references 12 and 13, respectively. Emissivity values for Teflon were obtained from reference 14. The values of $c_{p,l}$ were obtained from reference 15. The values of T_w/T_l and $c_{p,c}/c_{p,l}$ were 0.498 and 0.93 for the ethylene-jet test and equal to 0.167 and 0.5 for the arc-jet test. Since the products formed by the depolymerization of Teflon are a gas, f is equal to 1. In some static tests, a liquid phase has been observed; however, in computing the values shown in figure 8, f equal to 1 was used.

The vertical lines shown in figure 8 represent the data of reference 16. No values of T_w/T_l and $c_{p,c}/c_{p,l}$ were available for the data of reference 16. However, reference 16 uses $\left(M_{air}/M_{gas}\right)^{1/4}$ to correlate the results for different material vapors; thus, it was assumed that the ratio $c_{p,c}/c_{p,l}\left/\left(T_w/T_l\right)^{0.19}\right.$ was 0.76 (the value of $\left(M_{air}/M_{gas}\right)^{1/4}$ for Teflon). Thus, the enthalpy potential values of reference 16, $H_{aw} - H_{w,air}$, were multiplied by 0.76 to conform to the parameters of figure 8. It should be noted that the data of reference 16, as shown in figure 8, would give an intercept value 900 Btu/lb (calculated value of h_{ov} for Teflon) instead of 750 Btu/lb as shown in reference 16.

Downstream Cooling Effect of Ablating Materials

A problem related to ablation cooling for which solutions are obtained by essentially the same procedure as described in the previous

sections is that of the downstream cooling effect on a solid surface behind an ablating material. In downstream cooling, the coolant is ejected into the boundary layer forward of the surface which is to be cooled and is swept back over the rearward section by the air flow. In the following sections it will be shown how the temperature distribution results on a nonporous plate behind a region with transpiration cooling can be correlated in terms of the parameters pertaining to ablation cooling.

Two-dimensional laminar compressible flow.- In figure 11, there are shown the results of the analysis of reference 17 for the temperature distribution on an insulated nonporous plate behind a region with transpiration cooling. The results are given in terms of the wall cooling efficiency parameter $(T_w - T_c)/(T_{aw} - T_c)$ as a function of the distance behind a porous region for a number of fixed flow rates. A family of curves is obtained by this procedure, each curve pertaining only to a certain flow rate. Since x represents the sum of the porous and downstream areas and x_o represents the porous area, the quantity $(x/x_o - 1)$ is equal to S_ξ/S_p, which is the ratio of the downstream cooled area to that of the porous area.

Since, by definition

$$-f_o = \frac{G}{S_p}\sqrt{N_{Re,\infty}}$$

where G is the nondimensional flow rate averaged over the area of injection, $\bar{\dot{m}}/(\rho V)_l$, the term

$$\frac{-f_o}{\frac{x}{x_o} - 1} = \frac{\frac{G}{S_p\sqrt{N_{Re,\infty}}}}{S_\xi/S_p} = \frac{G}{S_\xi\sqrt{N_{Re,\infty}}} = F_\xi\sqrt{N_{Re,\infty}}$$

Dividing by $N_{St,aero,\xi}\sqrt{N_{Re,\infty}}$ (ref. 18) gives the downstream flow-rate correlation parameter

$$\left(\frac{F}{N_{St,aero}}\right)_\xi$$

The single correlation curve obtained by this procedure is shown in figure 12. The values of $(F/N_{St,aero})_\xi$ were multiplied by the ratio $c_{p,c}/c_{p,l}$. This permits application of the results to any coolant. (See appendix.)

Two-dimensional turbulent compressible flow.- Also shown in figure 12 are the faired experimental results of reference 19. These results were derived from tests conducted with a two-dimensional wing segment having constant chord thickness. The wing segment was constructed with a semicircular porous leading edge through which helium was ejected. The tests were conducted in a Mach number 2.0 ethylene-heated high-temperature air jet for stagnation temperatures ranging from 500° F to 2,400° F and for angles of attack of 0°, ±5°, and ±15°.

Correlation in terms of ablation cooling.- Since

$$\left(\frac{F}{N_{St,aero}}\right)_{\xi} \frac{c_{p,c}}{c_{p,l}} \equiv \frac{G/S_{\xi}}{N_{St,aero,\xi}} \frac{c_{p,c}}{c_{p,l}} \equiv \frac{G/S_p}{N_{St,aero,p}} \frac{S_p}{S_{\xi}} \frac{N_{St,aero,p}}{N_{St,aero,\xi}} \frac{c_{p,c}}{c_{p,l}}$$

then

$$\left(\frac{F}{N_{St,aero}}\right)_{\xi} \frac{c_{p,c}}{c_{p,l}} = \left(\frac{F}{N_{St,aero}}\right)_{p} \frac{c_{p,c}}{c_{p,l}} \frac{S_p}{S_{\xi}} \frac{N_{St,aero,p}}{N_{St,aero,\xi}}$$

where the factor $\left(F/N_{St,aero}\right)_p$ is the flow-rate correlation parameter for the area of injection. Since,

$$\frac{F}{N_{St,aero}} = \frac{f\left(H_{aw} - H_{w,air}\right)}{h_{eff}}$$

the downstream flow-rate correlation parameter can be written as

$$\left(\frac{F}{N_{St,aero}}\right)_{\xi} = \left[\frac{f\left(H_{aw} - H_{w,air}\right)}{h_{eff}}\right]_{le} \left(\frac{c_{p,c}}{c_{p,l}}\right)\left(\frac{S_{le}}{S_{\xi}}\right)\left(\frac{N_{St,aero,le}}{N_{St,aero,\xi}}\right) \tag{7}$$

and, thus, directly applies when ablating materials are used at the leading edge.

Since the quantity G is an average value over the injection area, the average mass loss rate $\dot{m}$ is determined from

$$\bar{\dot{m}} = \frac{\overline{q_{aero,le}}}{h_{eff,le}} \tag{8}$$

and is an average value for the portion of the leading-edge area which is supplying the vaporized mass that cools the downstream surface. The coolant temperature T_c which is the temperature of the ejected coolant at the junction of the injection and downstream areas becomes the vaporization temperature T_{vap} or the sublimation temperature T_{sub} depending on whether the material melts and vaporizes or directly sublimes. For the case where the material directly sublimes ($f = 1.0$), the use of figure 12 is straightforward. The material h_{eff} at the leading edge is calculated for $f = 1.0$ and $H_{w,air}$ equal to $c_{p,l}T_{sub}$. The downstream flow-rate correlation parameter is then computed for the various downstream positions and T_ξ is consequently determined from the curves of figure 12. For the case of melting vaporization where all the melt vaporizes at the leading edge ($f = 1.0$), the procedure is the same as for the sublimation case, except $H_{w,air}$ is now equal to $c_{p,l}T_{vap}$.

For the case where f is less than 1, some of the melt flows back over the afterbody, the length of melt depending on the melt heat capacity and the heat input into the melt as it flows along the afterbody. In this case, the downstream cooling procedure for $f = 1.0$ is applied at the position where the melt terminates. The afterbody surface that is covered by the melt is at a temperature that is essentially equal to the temperature of the underside of the melt.

The circular symbols shown in figure 12 are the experimental results obtained from a series of tests conducted in a Mach number 4.0 ceramic-heated jet. The test configuration was a 5/8-inch-diameter hemisphere-cylinder. The cylindrical section was approximately $2\frac{1}{2}$ inches long and constructed from 1/16-inch-thick Inconel. The hemispherical cap was Teflon material. The Inconel section was instrumented with thermocouples. The details of these tests are given in reference 20. Unfortunately, reference 20 presents only the value of $\dot{m}$ at the stagnation point, and does not provide the experimental information to obtain $\bar{\dot{m}}$ from equation (8). However,

$$\left(\frac{F}{N_{St,aero}}\right)_\xi = w\left(\frac{c_{p,c}}{h_o S}\right)_\xi$$

where w is the total weight loss of the nose material per second, and $c_{p,c,\xi}$, $h_{o,\xi}$, and S_ξ are the specific heat of the nose material vapor,

heat-transfer coefficient, and cooled area of the downstream position. The values of w were obtained from Douglas Aircraft Company, Inc.; the values of T_c $\left(T_c \equiv T_w\right)$ and $c_{p,c}$, from figures 9 and 10; the values of T_ξ, from extrapolation of the temperature data of reference 20 by means of a plot of $\log T$ against $1/\tau$.

It should be noted that the afterbody surface temperatures shown in figure 12 are steady-state or equilibrium values. For the case where the afterbody surface is wetted by the coolant but has not as yet reached steady-state temperatures, the temperature during the transient period is given by the following equation:

$$\frac{T - T_c}{T_{aw} - T_c} = \frac{T_\xi - T_c}{T_{aw} - T_c} - \frac{\left(\rho c_p t\right)_w \left(\frac{dT}{d\tau}\right)_\xi}{h_{o,\xi}\left(T_{aw} - T_c\right)\left[\left(\frac{N_{St}}{N_{St,aero}}\right)_\xi + \left(\frac{F}{N_{St,aero}}\right)_\xi \frac{c_{p,c}}{c_{p,l}}\right]} \tag{9}$$

The values of $\left(N_{St}/N_{St,aero}\right)_\xi$ are shown in figure 13 for both the laminar and turbulent cases as a function of the parameter

$$\left(\frac{F}{N_{St,aero}}\right)_\xi \frac{c_{p,c}}{c_{p,l}} = f\left(\frac{H_{aw} - H_{w,air}}{h_{eff}}\right)_{le} \frac{S_{le}}{S_\xi} \frac{N_{St,aero,le}}{N_{St,aero,\xi}} \frac{c_{p,c}}{c_{p,l}}$$

Radiation effects are accounted for by correcting the term $h_{o,\xi}$. Since

$$q_o = q_{aero} - q_{rad}$$

or

$$h_o\left(T_{aw} - T_w\right) = h_{aero}\left(T_{aw} - T_w\right) - \sigma\epsilon T_w^4$$

there results

$$h_o = h_{aero} - \frac{\sigma\epsilon T_w^4}{\left(T_{aw} - T_w\right)}$$

or for the downstream surface

$$h_{o,\xi} = h_{aero,\xi} - \frac{\sigma \epsilon T_{w,\xi}^{4}}{\left(T_{aw} - T_{w}\right)_{\xi}}$$

CONCLUSIONS

The following conclusions are based on the results obtained from an analytical investigation of ablation cooling:

1. Effective heat of ablation relationships for several types of boundary layers applicable for all wall-to-local temperature ratios can be derived simply and directly from transpiration cooling results.

2. The predicted effective heats of ablation for a three-dimensional laminar stagnation boundary layer for Teflon material are in agreement with those derived from tests conducted at boundary-layer enthalpy potentials of 800 and approximately 7,000 Btu/lb.

3. The predicted equilibrium surface temperatures on nonablating surfaces behind an ablating material are in agreement with the values derived from tests conducted with Inconel cylinders having Teflon hemispherical nose shapes.

Langley Research Center,
National Aeronautics and Space Administration,
Langley Field, Va., April 25, 1960.

APPENDIX

DERIVATION OF THE CORRELATION PARAMETER $c_{p,c}/c_{p,l}$

In the sections dealing with the derivations of the shielding expressions, it was indicated that the parameter

$$\left(\frac{F}{N_{St,aero}}\right)\left(\frac{c_{p,c}}{c_{p,l}}\right)$$

(where $c_{p,c}$, the coolant or vapor specific heat, was evaluated at the cooled wall temperature and $c_{p,l}$, the local stream specific heat, was evaluated at the temperature of the outer edge of the boundary layer) essentially correlated all the cooling results regardless of the type of coolant used.

For the case of foreign gas ejection, the gas layer adjacent to the cooled surface is made up of both molecules of foreign gas and the local stream. The specific-heat capacity of this mixture will be denoted as $c_{p,m}$ and is defined

$$c_{p,m} = Wc_{p,c} + (1 - W)c_{p,w}$$

where W is the mass fraction of the foreign gas evaluated at the wall and $c_{p,w}$ is the local stream specific heat evaluated at the wall temperature. Thus

$$\frac{c_{p,m}}{c_{p,l}} = W\frac{c_{p,c}}{c_{p,l}} + (1 - W)\frac{c_{p,w}}{c_{p,l}}$$

and

$$\frac{c_{p,m}}{c_{p,c}} = \frac{c_{p,m}/c_{p,l}}{c_{p,c}/c_{p,l}}$$

Reference 21 gives theoretical results for W as a function of f_w for hydrogen-to-air cooling for both the two- and three-dimensional

laminar stagnation cases. Reference 22 gives results for the hydrogen-to-air cooling of a two-dimensional laminar layer. Reference 23 gives results for the helium-to-air cooling of a two-dimensional laminar layer. The results of these references are given in figure 14 where $c_{p,m}/c_{p,c}$ is plotted against $F/N_{St,aero}$ (f_w is analogous to this parameter). The results indicate that for the four cases shown, $c_{p,m}/c_{p,c}$ becomes equal to 1.0 when $F/N_{St,aero}$ is greater than 0.7. Thus, since

$$\frac{F}{N_{St,aero}} = \frac{f\left(H_{aw} - H_{w,air}\right)}{h_{eff}}$$

the generalization of the ablation formulas to all types of vapors, through use of the factor $c_{p,c}/c_{p,l}$, is probably very good when

$$f\left(H_{aw} - H_{w,air}\right) > h_{eff}$$

For steady-state or equilibrium conditions (radiation and conduction assumed negligible), the heat balance equation for transpiration cooling is

$$\frac{N_{St}}{N_{St,aero}} = \frac{F}{N_{St,aero}} \frac{c_{p,m}}{c_{p,l}} \frac{\left(T_w - T_c\right)}{\left(T_e - T_w\right)}$$

or in view of the preceding argument

$$\frac{N_{St}}{N_{St,aero}} = \frac{F}{N_{St,aero}} \frac{c_{p,c}}{c_{p,l}} \frac{\left(T_w - T_c\right)}{\left(T_e - T_w\right)}$$

where T_e is the boundary-layer recovery temperature for the mixture of coolant and stream flows and is defined as

$$T_e = T_c + \eta_e\left(T_t - T_c\right)$$

The term η_e is the temperature recovery factor and is defined as

$$\eta_e = \frac{T_e - T_c}{T_t - T_c}$$

reference 9 gives experimentally determined values of η_e for both air-to-air and helium-to-air transpiration cooling of a two-dimensional turbulent boundary layer as a function of the flow-rate parameter $F/N_{St,aero}$. The results of reference 9 were modified by multiplying $F/N_{St,aero}$ by the ratio $c_{p,c}/c_{p,l}$ and plotting η_e as a function of $\left(F/N_{St,aero}\right)\left(c_{p,c}/c_{p,l}\right)$. This plot is shown in figure 15 and it is seen that η_e is essentially linear with $\left(F/N_{St,aero}\right)\left(c_{p,c}/c_{p,l}\right)$ and can be expressed by the relationship

$$\eta_e = \eta_{aw} - 0.015\left(\frac{F}{N_{St,aero}}\right)\left(\frac{c_{p,c}}{c_{p,l}}\right)$$

where η_{aw} is the temperature recovery factor for no mass transfer.

Thus, for the same T_w and T_c (coolant storage temperature), the ratio $N_{St}/N_{St,aero}$ is only a function of $\left(F/N_{St,aero}\right)\left(c_{p,c}/c_{p,l}\right)$ since T_e is also specified by this ratio.

In correlating the experimental results of references 8, 9, and 19, $c_{p,l}$ was evaluated for the temperature at the outer edge of the boundary layer. At high temperatures, however, the $c_{p,l}$ varies considerably with small changes in temperature and pressure. In order that the calculations be not incorrectly influenced by these variations, the $c_{p,l}$ which was used at high values of enthalpy potential was the average specific heat for the temperature range through the boundary layer. This average value was calculated from

$$c_{p,l} = \frac{H_l - H_w}{T_l - T_w}$$

REFERENCES

1. Rashis, Bernard, Witte, William G., and Hopko, Russell N.: Qualitative Measurements of the Effective Heats of Ablation of Several Materials in Supersonic Air Jets at Stagnation Temperatures Up to 11,000° F. NACA RM L58E22, 1958.

2. Casey, Francis W., Jr., and Hopko, Russell N.: Preliminary Investigation of Graphite, Silicon Carbide, and Several Polymer—Glass-Cloth Laminates in a Mach Number 2 Air Jet at Stagnation Temperatures of 3,000° F and 4,000° F. NACA RM L57K15, 1958.

3. Rashis, Bernard, and Walton, Thomas E., Jr.: An Experimental Investigation of Ablating Materials at Low and High Enthalpy Potentials. NASA TM X-263, 1960.

4. Lees, Lester: Similarity Parameters for Surface Melting of a Blunt-Nosed Body in a High Velocity Gas Stream. Rep. No. GM-TM-184 (Contract No. AF 18(600)-1190), Guided Missile Res. Div., The Ramo-Wooldridge Corp., July 29, 1957.

5. Roberts, Leonard: Stagnation-Point Shielding by Melting and Vaporization. NASA TR R-10, 1959.

6. Scala, Sinclaire M.: A Study of Hypersonic Ablation. Tech. Inf. Series No. R59SD438 (Contract No. AF 04(647)-269), Missile and Space Vehicle Dept., Gen. Elec. Co., Sept. 30, 1959.

7. Hartnett, J. P., and Eckert, E. R. G.: Mass Transfer Cooling With Combustion in a Laminar Boundary Layer. 1958 Heat Transfer and Fluid Mechanics Institute (held at Univ. of California), Stanford Univ. Press, June 1958, pp. 54-68.

8. Rashis, Bernard: Exploratory Investigation of Transpiration Cooling of a 40° Double Wedge Using Nitrogen and Helium as Coolants at Stagnation Temperatures of 1,295° to 2,910° F. NACA RM L57F11, 1957.

9. Leadon, B. M., and Scott, C. J.: Measurement of Recovery Factors and Heat Transfer Coefficients With Transpiration Cooling in a Turbulent Boundary Layer at M = 3.0 Using Air and Helium as Coolants. Res. Rep. No. 126 (Contract AF 18(600)-1226), Inst. Tech., Dept. Aero. Eng., Univ. of Minnesota, Feb. 1956.

10. Brown, W. Byron, and Donoughe, Patrick L.: Tables of Exact Laminar-Boundary-Layer Solutions When the Wall Is Porous and Fluid Properties Are Variable. NACA TN 2479, 1951.

11. Reshotko, Eli, and Cohen, Clarence B.: Heat Transfer at the Forward Stagnation Point of Blunt Bodies. NACA TN 3513, 1955.

12. Steg, Leo: Materials for Re-Entry Heat Protection of Satellites [Preprint] 836-59, presented at the Am. Rocket Soc. Semi-Annual Meeting (San Diego, Calif.), June 1959.

13. Siegel, J. C., and Muus, L. T.: Pyrolysis of Polytetrafluoroethylene. Presented at meeting of American Chem. Soc., Sept. 17, 1956.

14. Grenis, Albert F., and Wong, Anthony K.: The Total Normal Thermal Emissivity of Teflon, Kel-F, and Duroid 5600 at Elevated Temperatures. Rep. No. WAL TR 397.1/1, Watertown Arsenal Labs. (Watertown, Mass.), July 1958.

15. Hansen, C. Frederick: Approximations for the Thermodynamic and Transport Properties of High-Temperature Air. NACA TN 4150, 1958.

16. Georgiev, Steven, Hidalgo, Henry, and Adams, Mac C.: On Ablation for Recovery of Satellites. 1959 Heat Transfer and Fluid Mechanics Institute (held at Univ. of California), Stanford Univ. Press, June 1959, pp. 171-180. (Also available as Res. Rep. 47 (Contract AF 04(647)-278), AVCO Res. Lab., Mar. 6, 1959.)

17. Rubesin, Morris W., and Inouye, Mamoru: A Theoretical Study of the Effect of Upstream Transpiration Cooling on the Heat-Transfer and Skin-Friction Characteristics of a Compressible, Laminar Boundary Layer. NACA TN 3969, 1957.

18. Van Driest, E. R.: Investigation of Laminar Boundary Layer in Compressible Fluids Using the Crocco Method. NACA TN 2597, 1952.

19. Witte, William G., and Rashis, Bernard: An Experimental Investigation and Correlation of the Heat Reduction to Nonporous Surfaces Behind a Porous Leading Edge Through Which Coolant Is Ejected. NASA TM X-235, 1960.

20. Byham, C. E.: Materials Tests in NASA Pilot Model Ceramic Heated Air Jet Model DM-15. Rep. SM-27972 (Contract DA-30-069-ORD-1955), Douglas Aircraft Co., Inc., June 2, 1959.

21. Hayday, A. A.: Mass Transfer Cooling in a Steady Laminar Boundary Layer Near the Stagnation Point. 1959 Heat Transfer and Fluid Mechanics Institute (held at Univ. of California), Stanford Univ. Press, June 1959, pp. 156-170.

22. Eckert, E. R. G., Schneider, P. J., and Koehler, F.: Mass Transfer Cooling of a Laminar Air Boundary Layer by Injection of a Light-Weight Gas. Tech. Rep. No. 8 (Contract No. AF-18(600)-1226), Heat Transfer Lab., Univ. of Minnesota, Apr. 1956.

23. Baron, Judson R.: The Binary-Mixture Boundary Layer Associated With Mass Transfer Cooling at High Speeds. Tech. Rep. 160, Naval Supersonic Lab., M.I.T., May 1956.

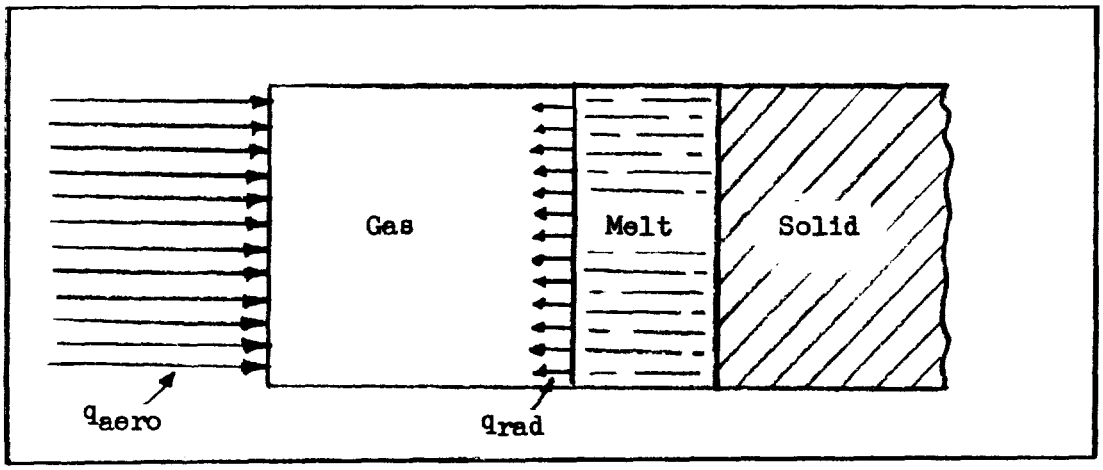

(a) Schematic diagram.

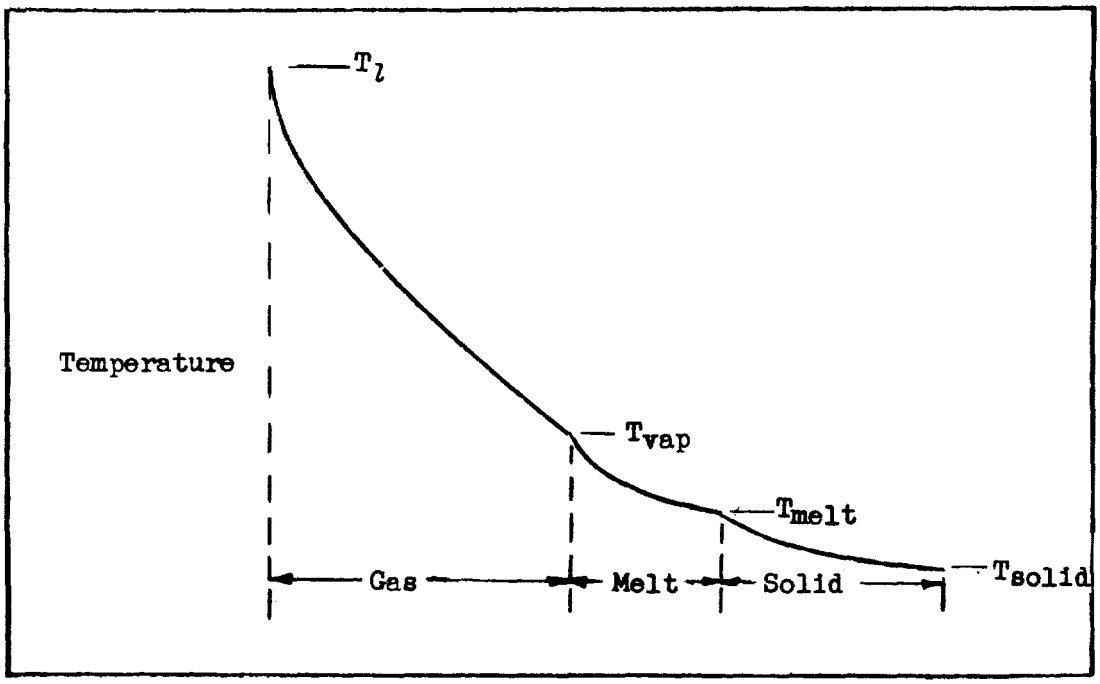

(b) Temperature distribution.

Figure 1.- Schematic diagram and temperature distribution of a melting-vaporizing body. Stagnation point.

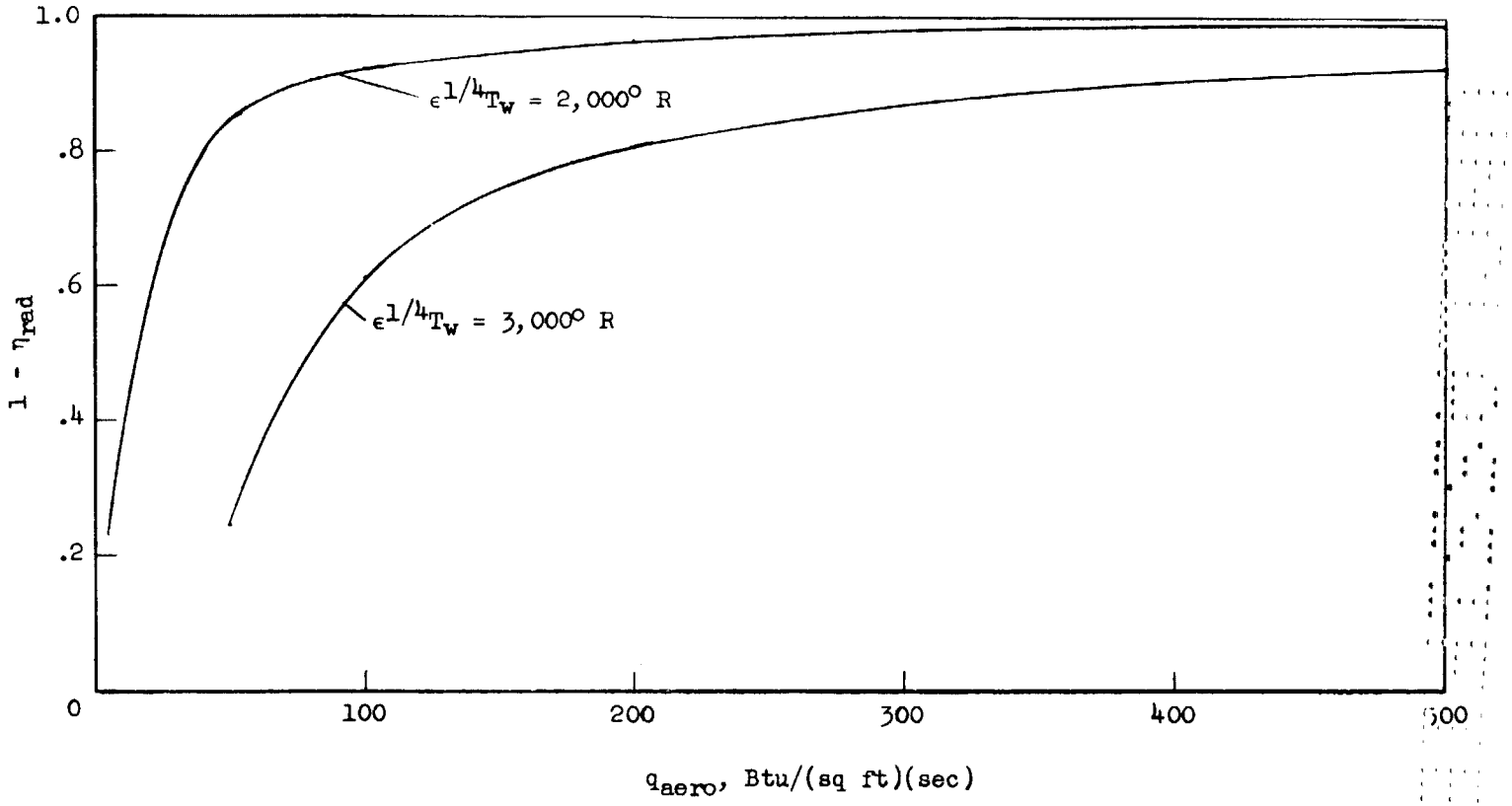

Figure 2.- Variation of radiation effect with aerodynamic heat flux and surface temperature.

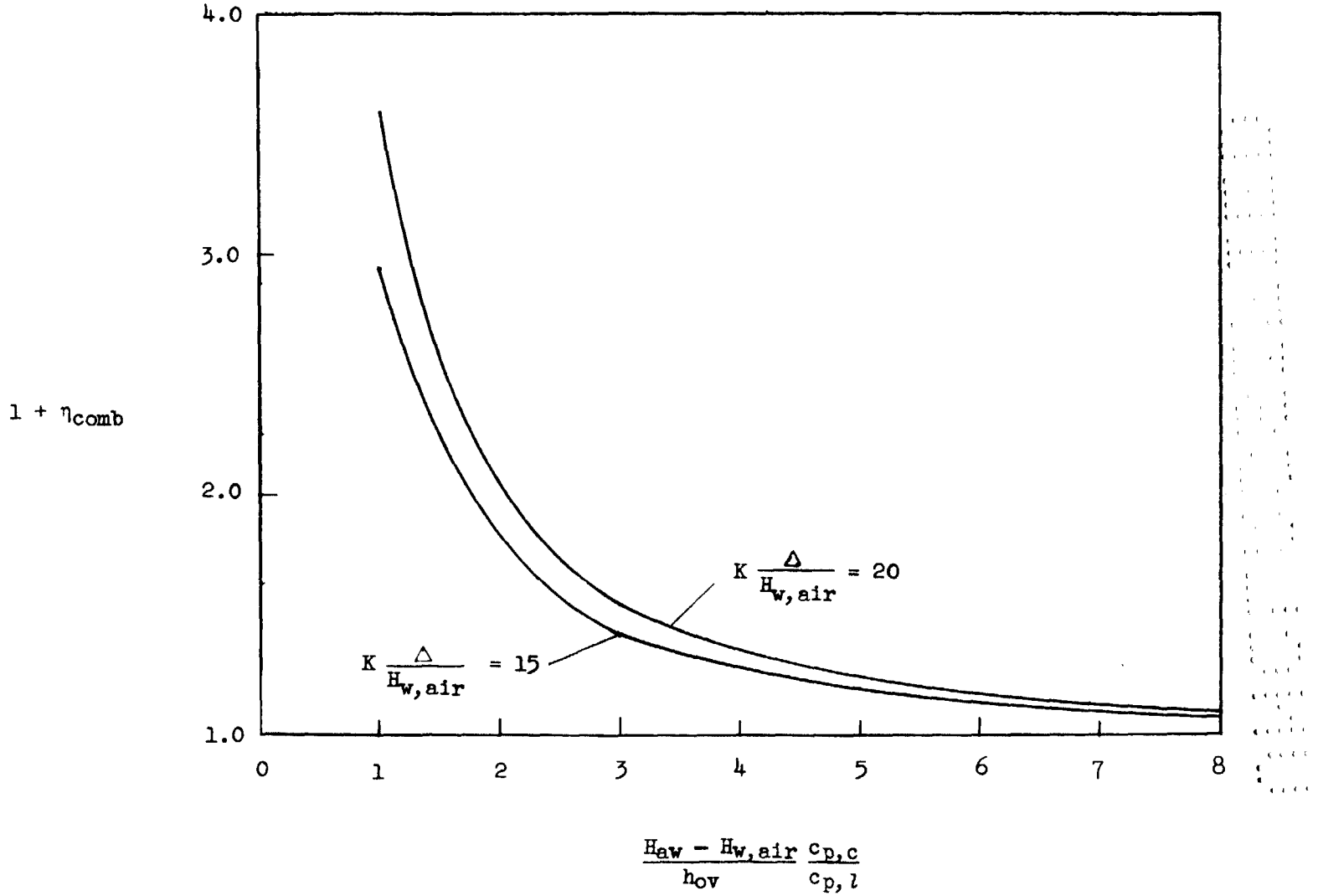

Figure 3.- Variation of combustion effect for an axially symmetric laminar boundary layer.

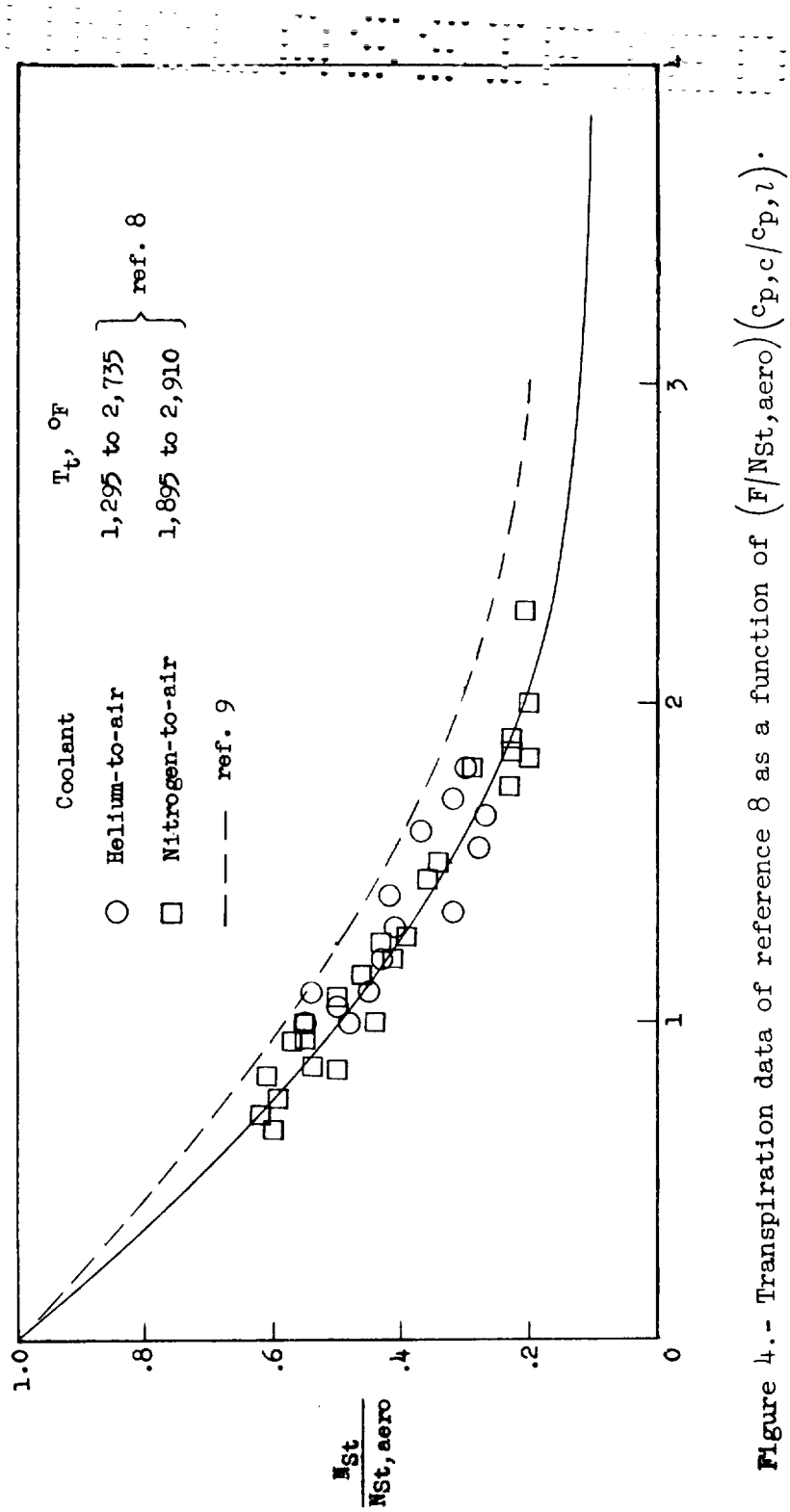

Figure 4.- Transpiration data of reference 8 as a function of $\left(F/N_{St,aero}\right)\left(c_{p,c}/c_{p,l}\right)$.

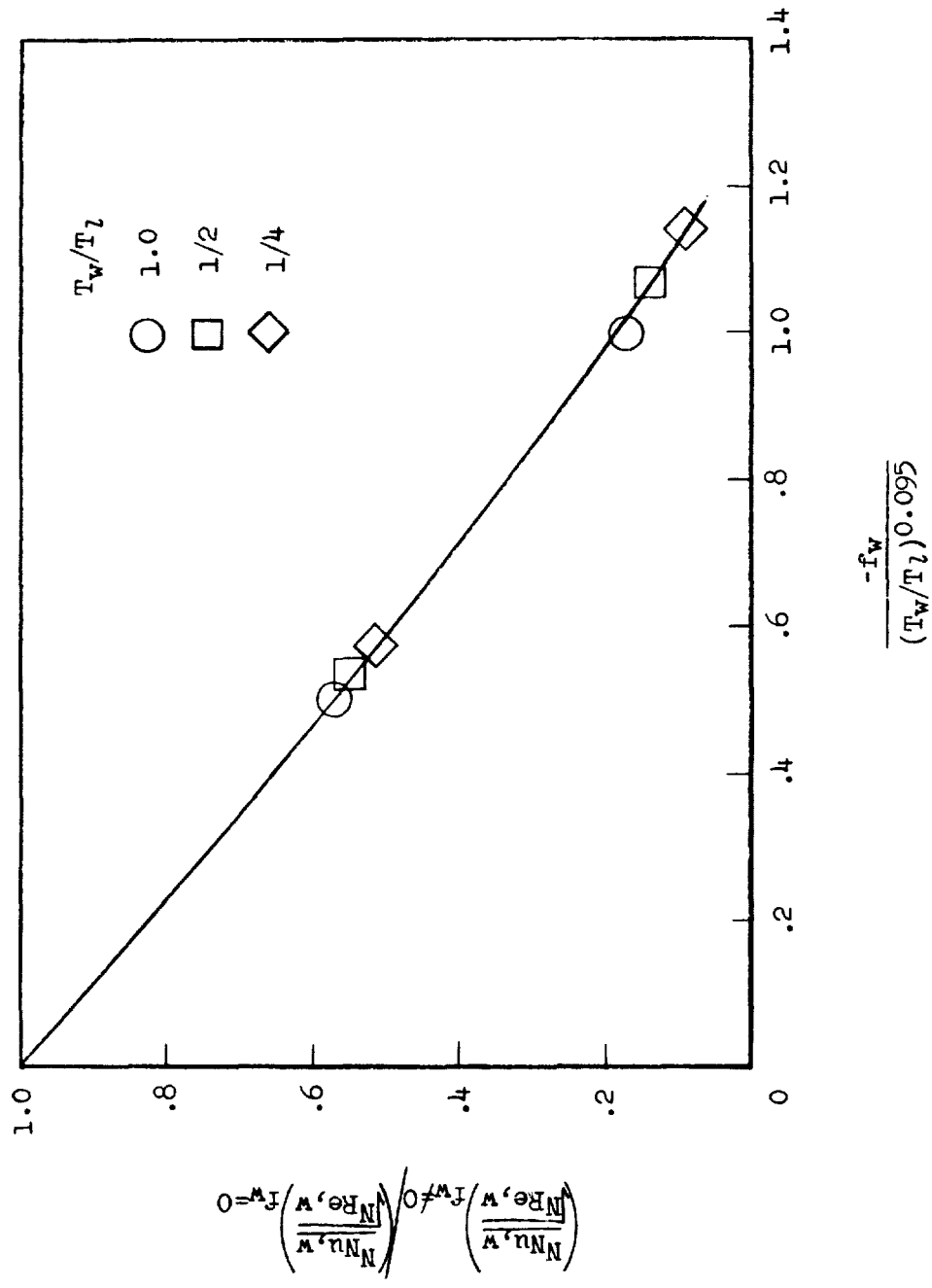

Figure 5.- Transpiration shielding results of reference 10 for a two-dimensional laminar boundary layer.

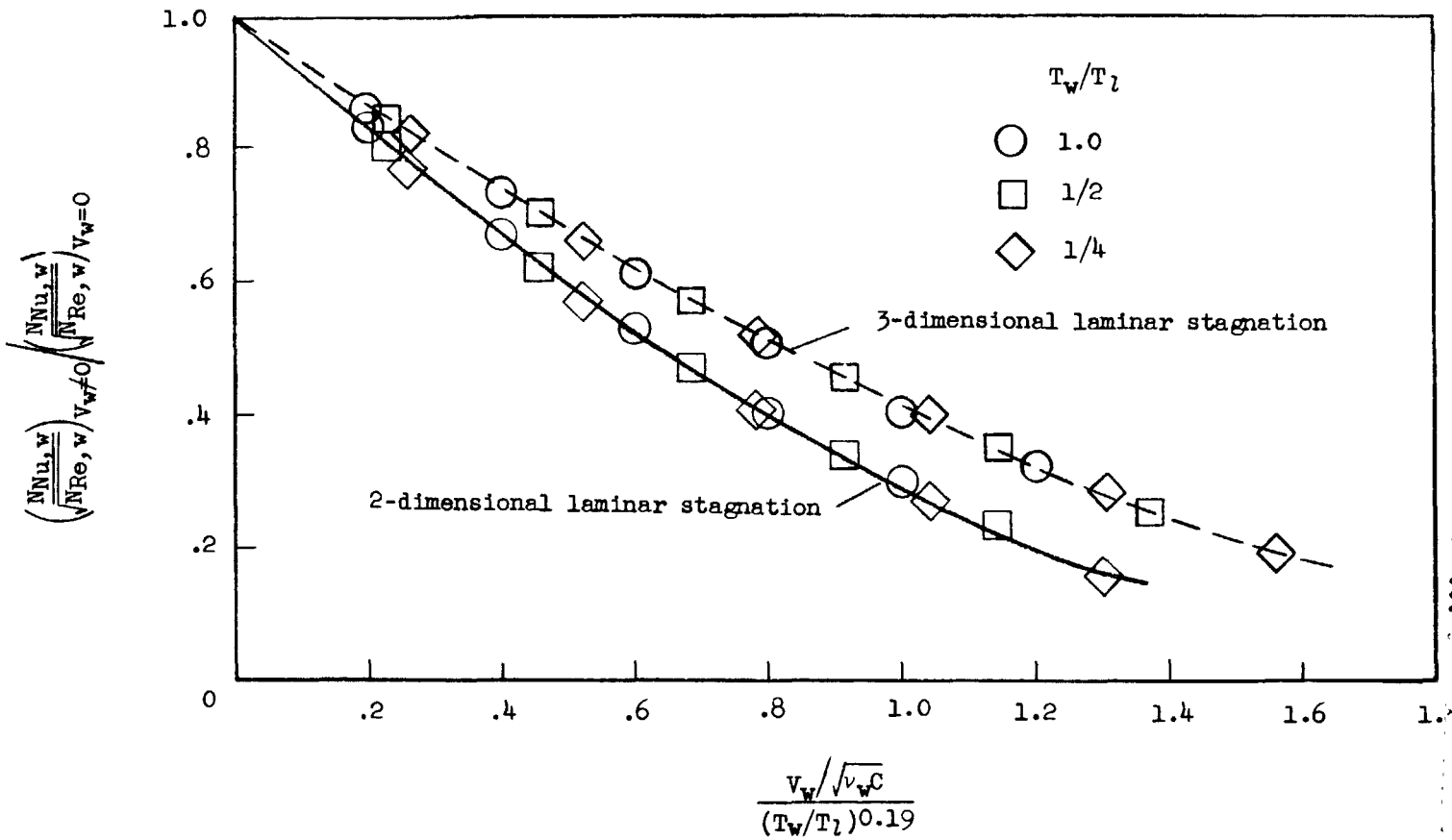

Figure 6.- Transpiration shielding results of reference 11 for two- and three-dimensional stagnation laminar boundary layers.

CONFIDENTIAL

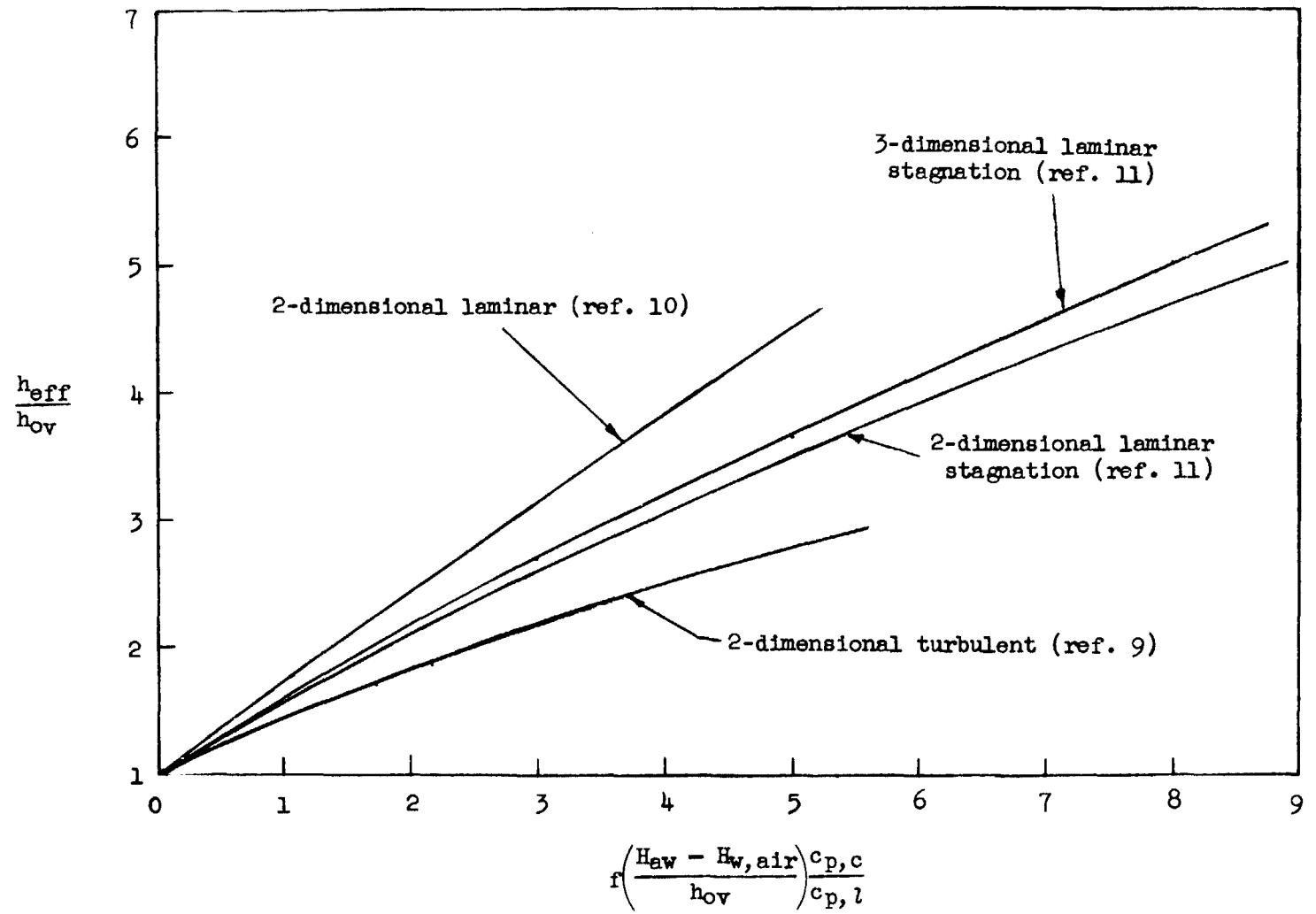

Figure 7.- Effective heats of ablation as a function of the ablating material and boundary-layer characteristics $T_w/T_l = 1$.

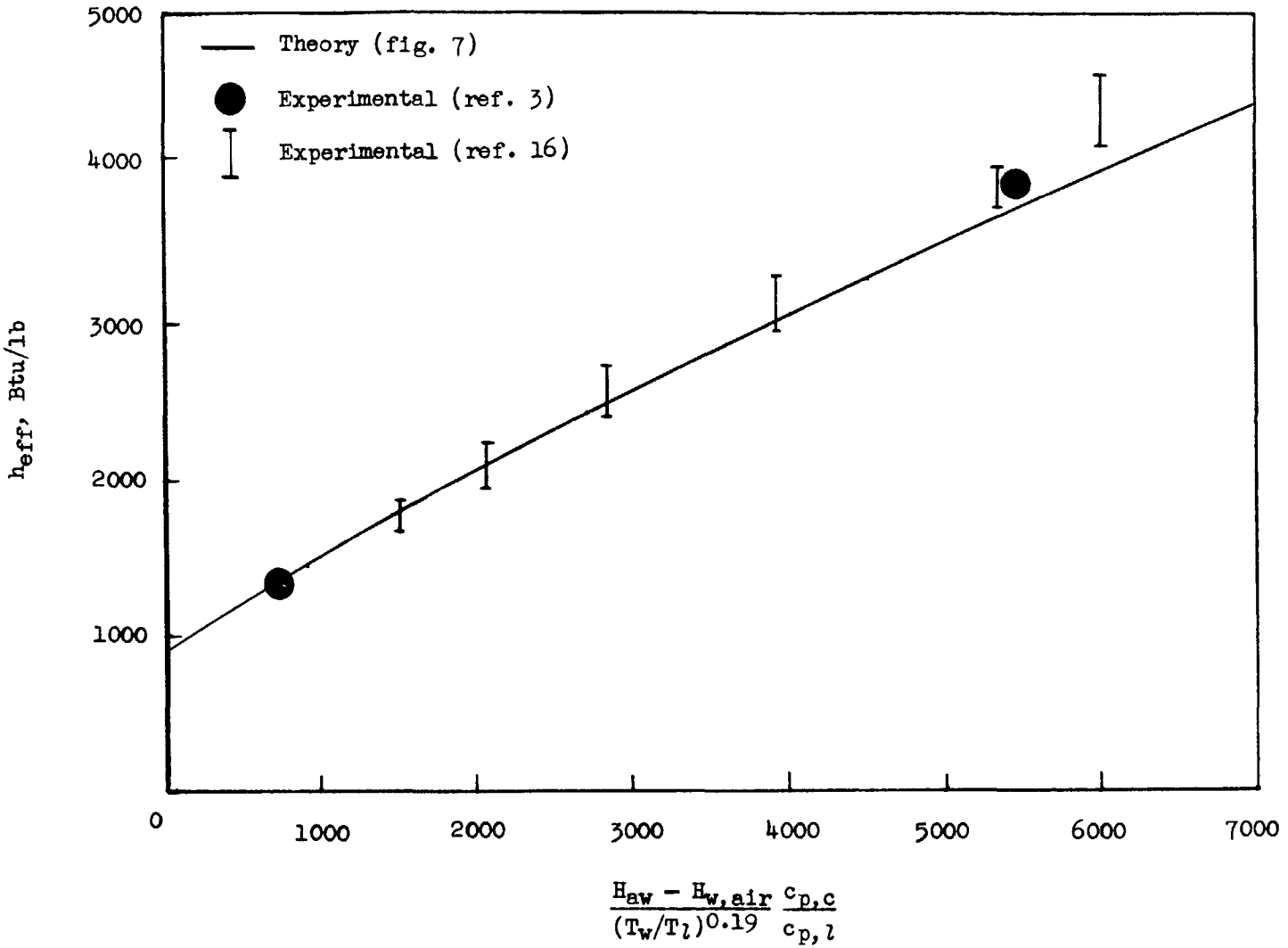

Figure 8.- Comparison of theory with experiment for Teflon.

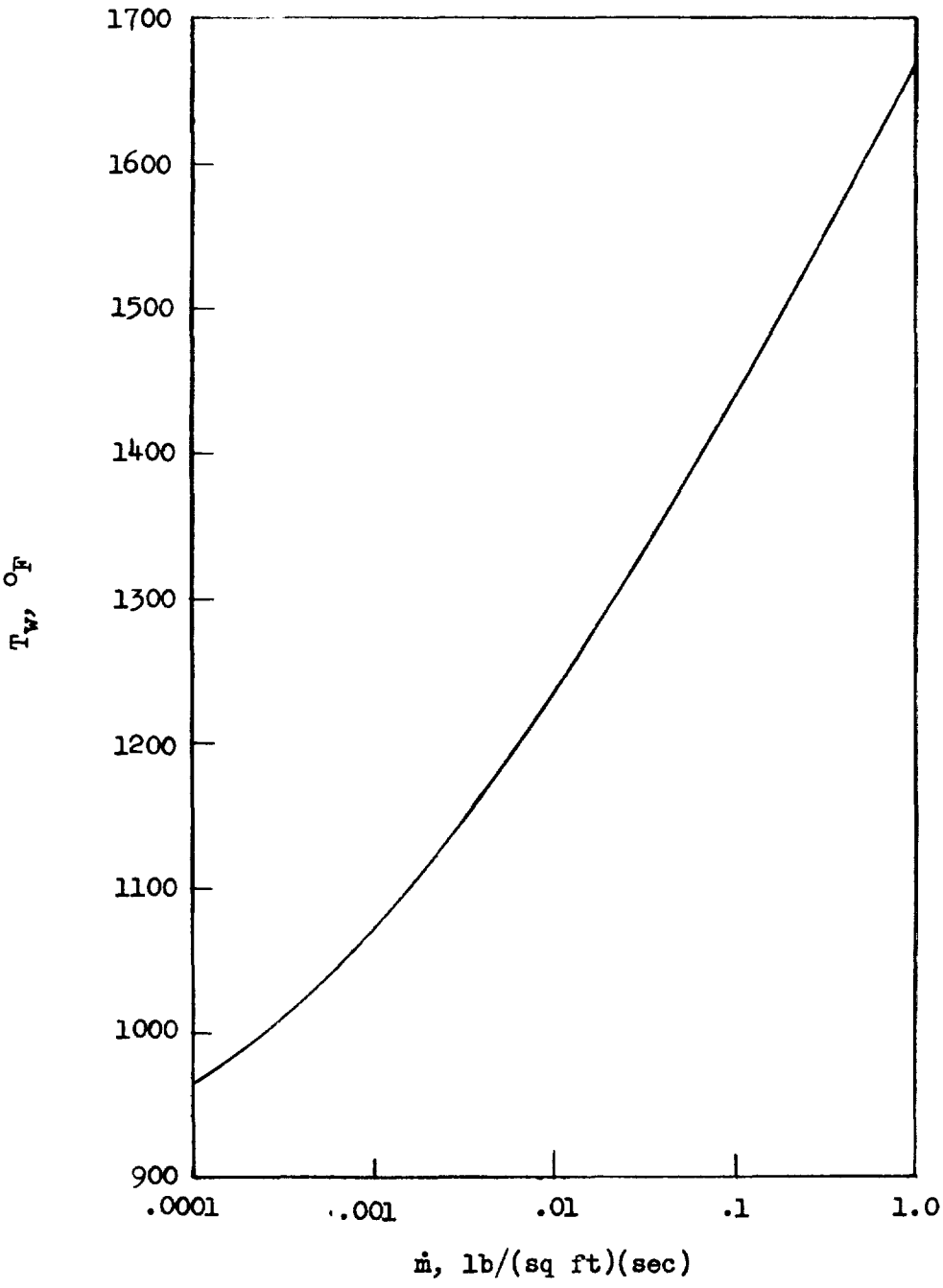

Figure 9.- Variation of surface temperature with ablation rate for Teflon. Reference 12.

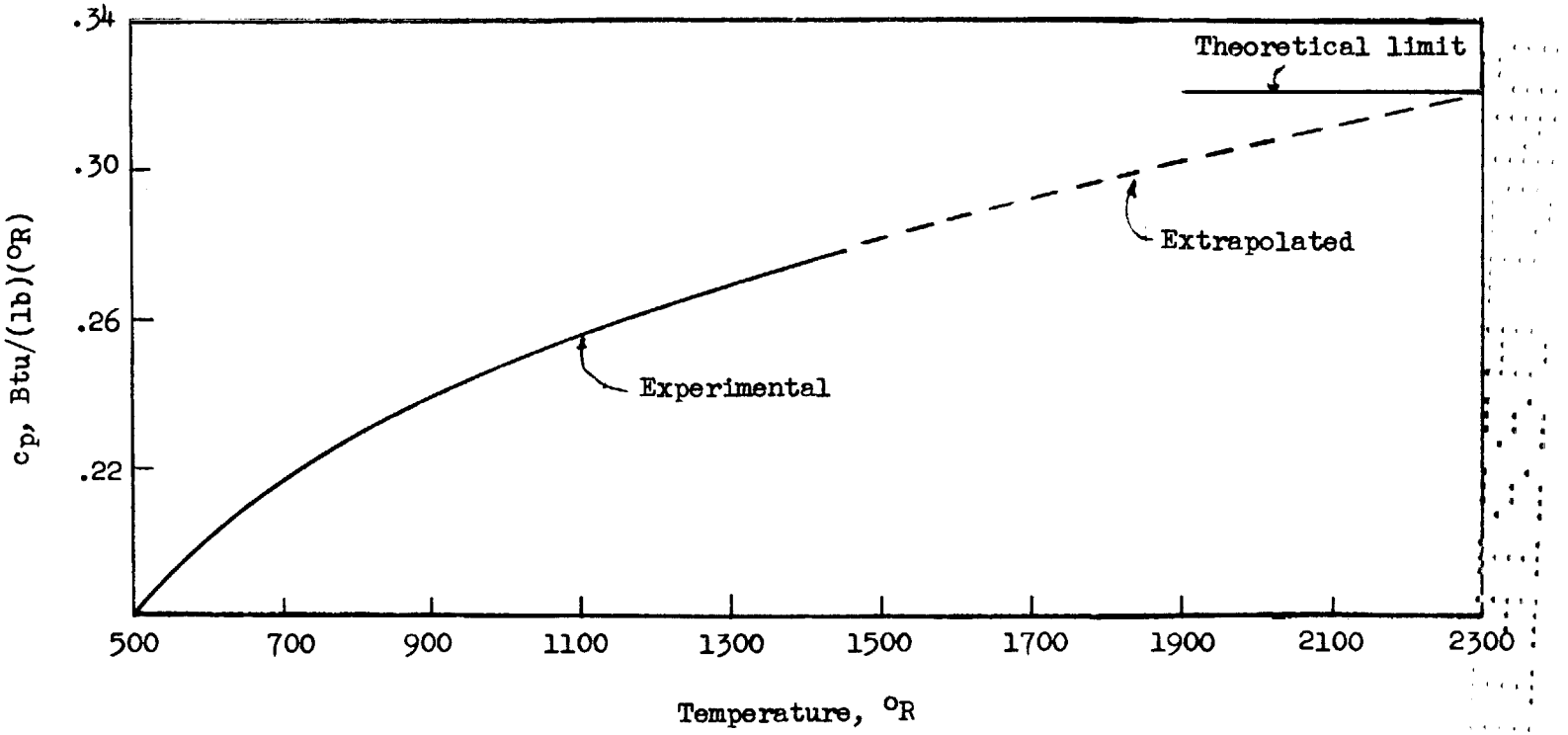

Figure 10.- Specific heat at constant pressure as a function of temperature for C_2F_4 vapor (Teflon monomer). Reference 13.

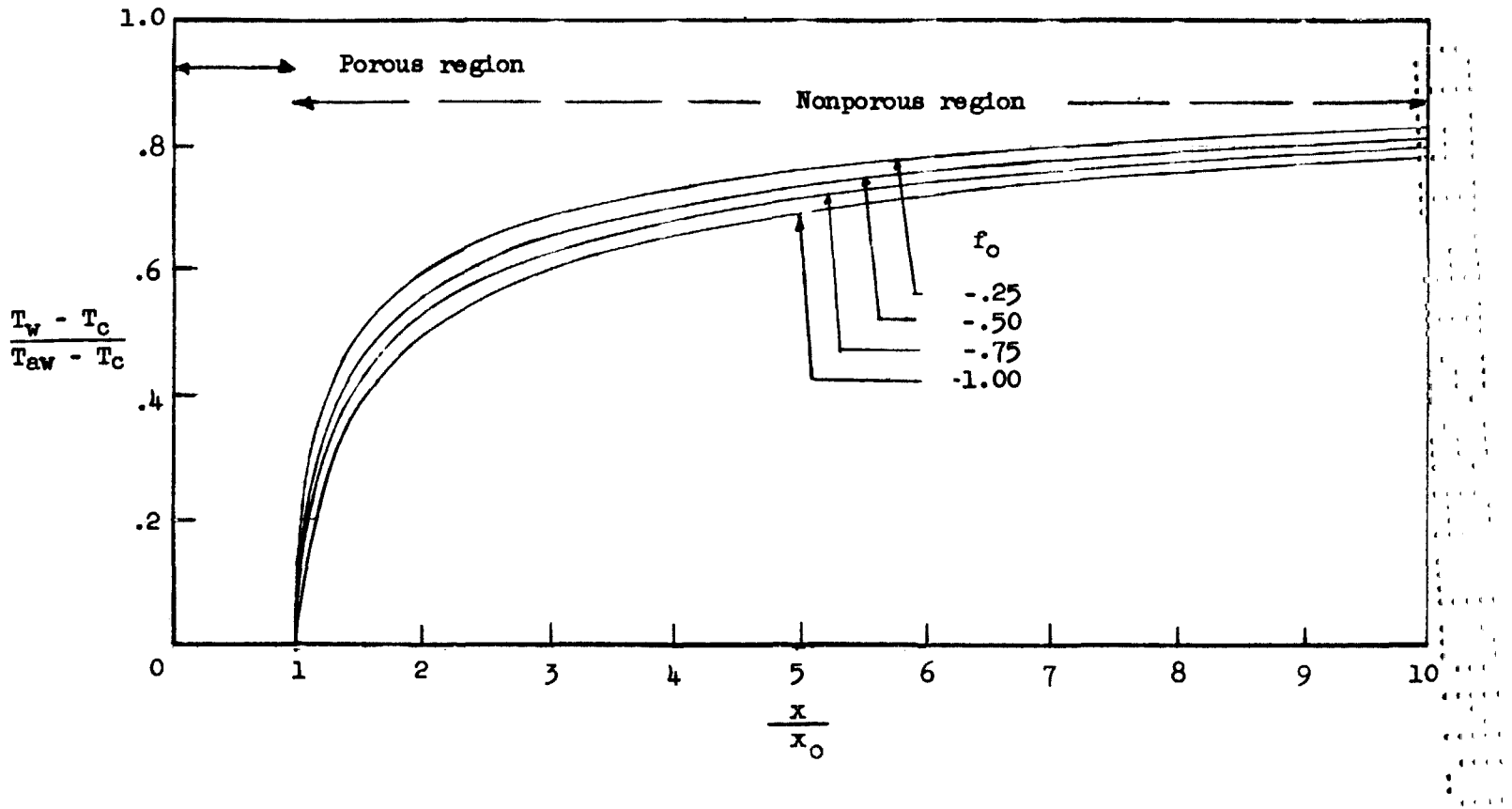

Figure 11.- Temperature distribution on an insulated nonporous plate behind a region with transpiration cooling. Reference 17.

CONFIDENTIAL

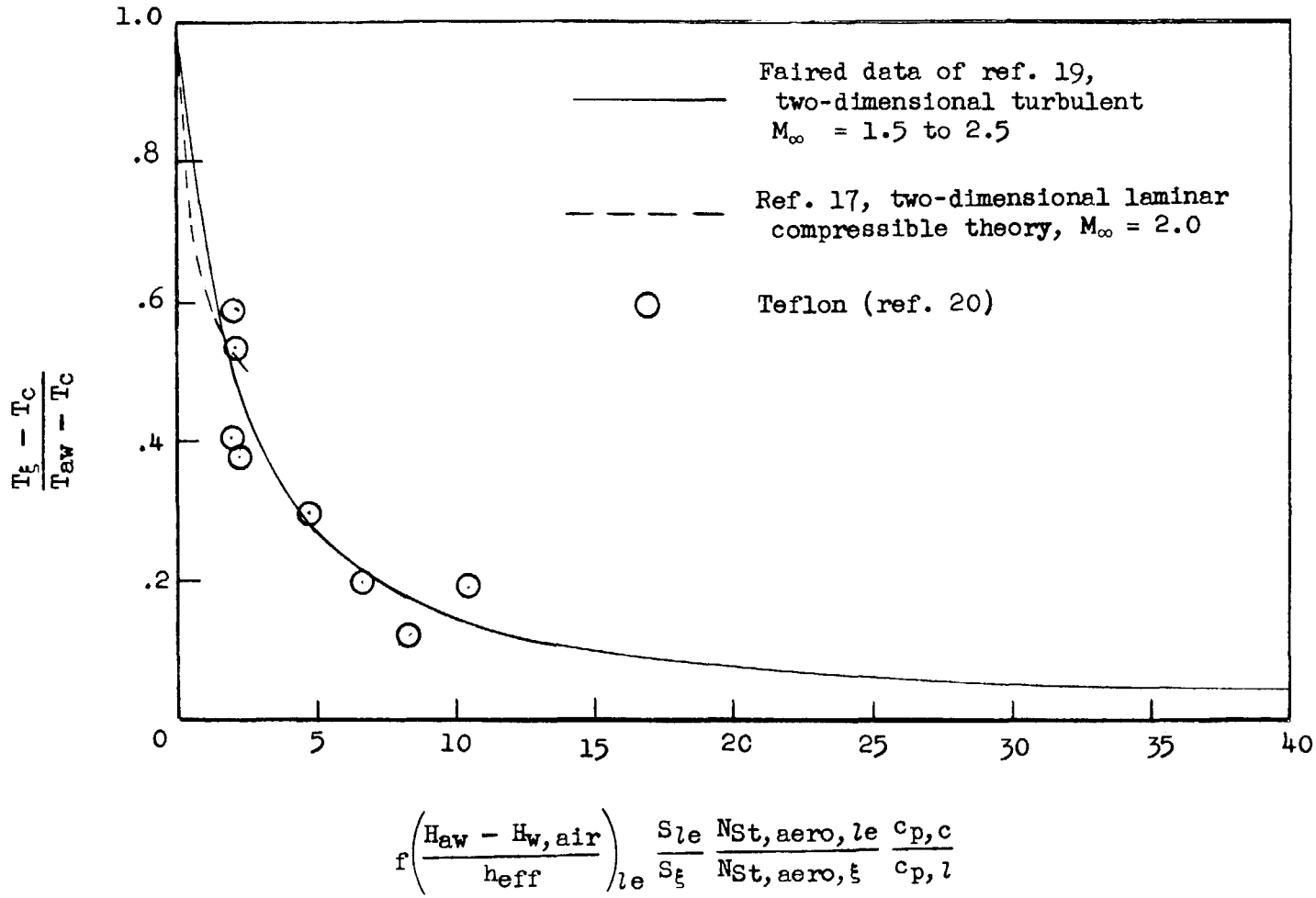

Figure 12.- Variation of downstream cooling as function of upstream ejection and cooled area.

CONFIDENTIAL

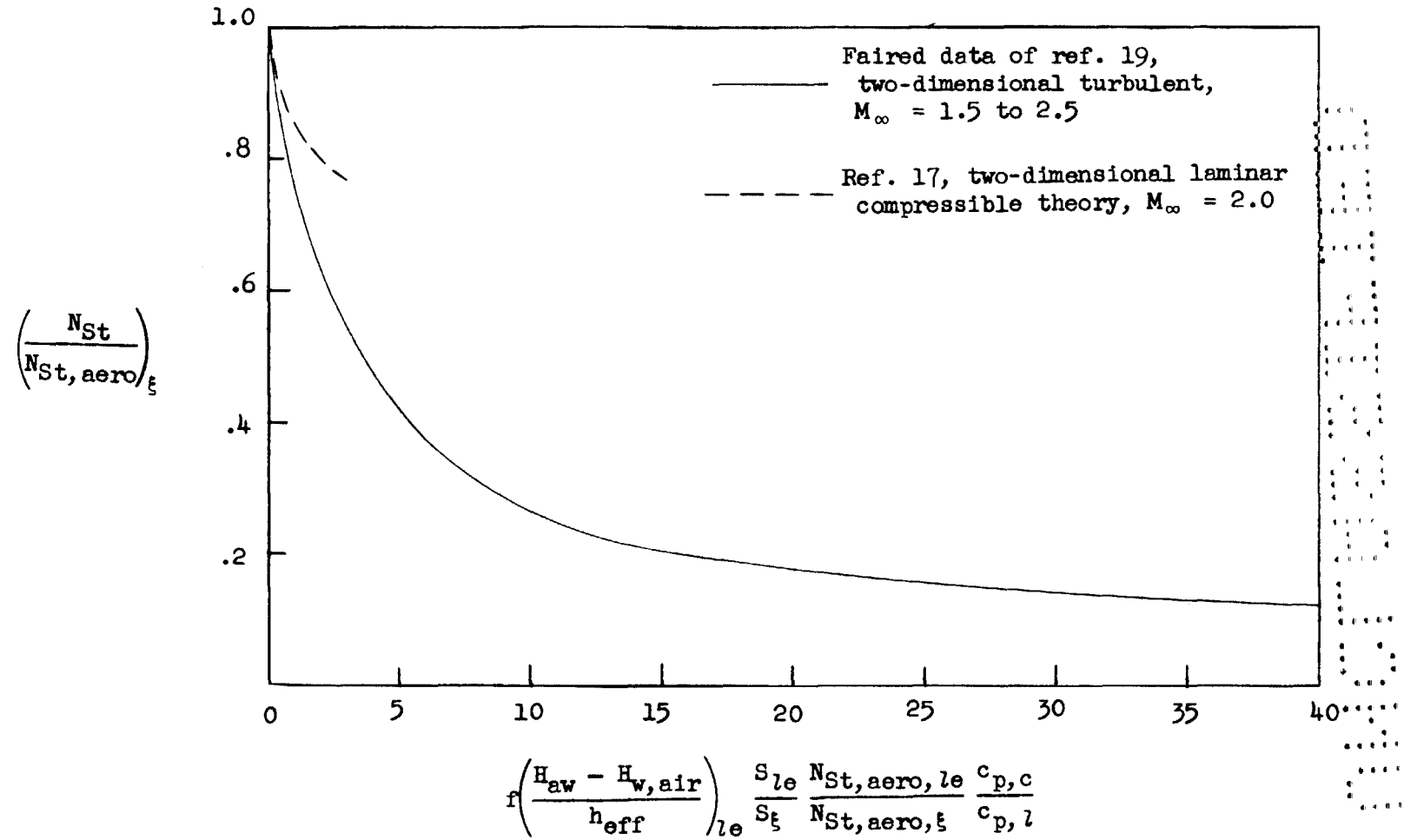

Figure 13.- Variation of heat reduction as function of upstream ejection and cooled area.

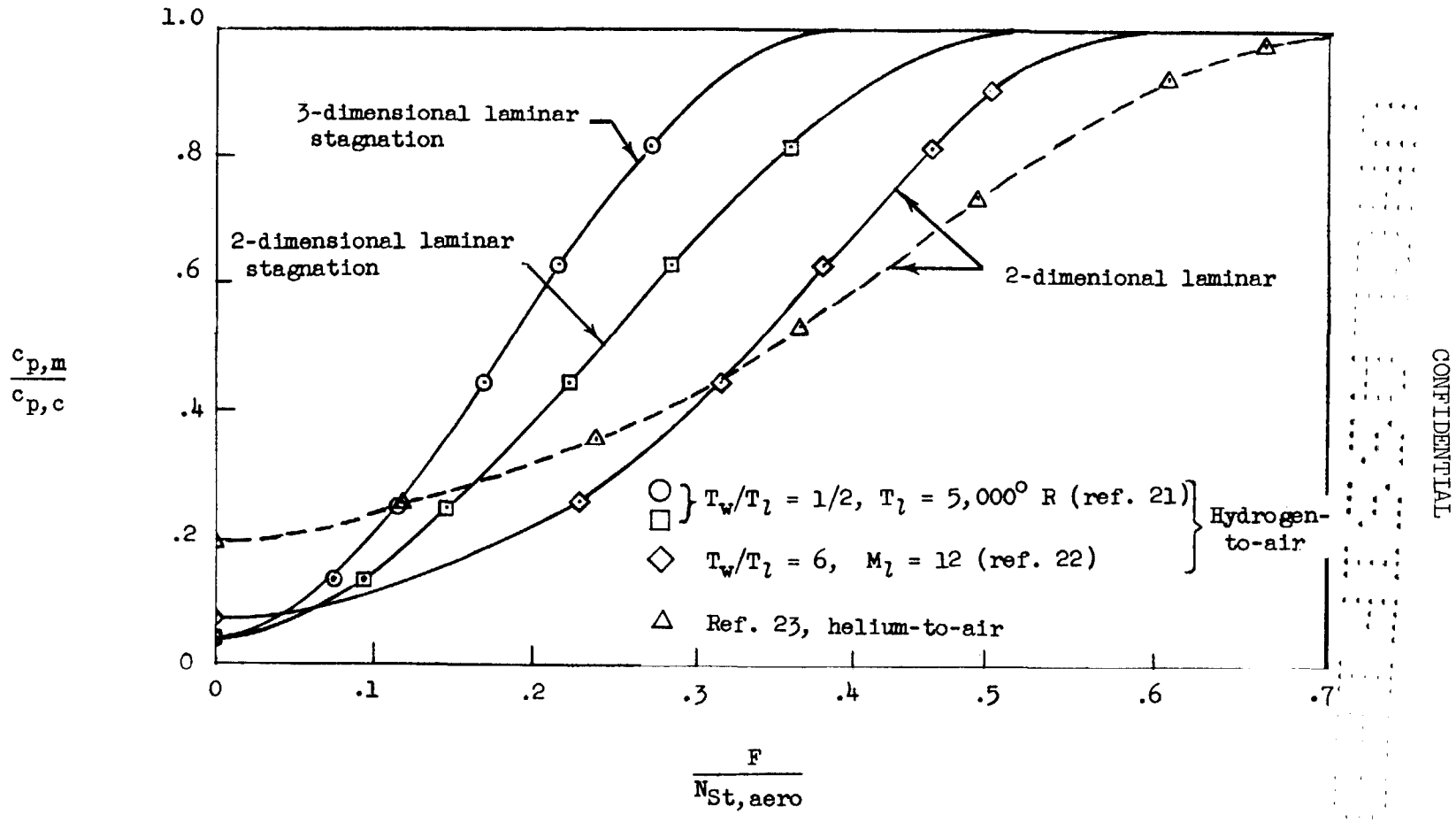

Figure 14.- Variation of mixture specific heat with flow-rate parameter.

CONFIDENTIAL

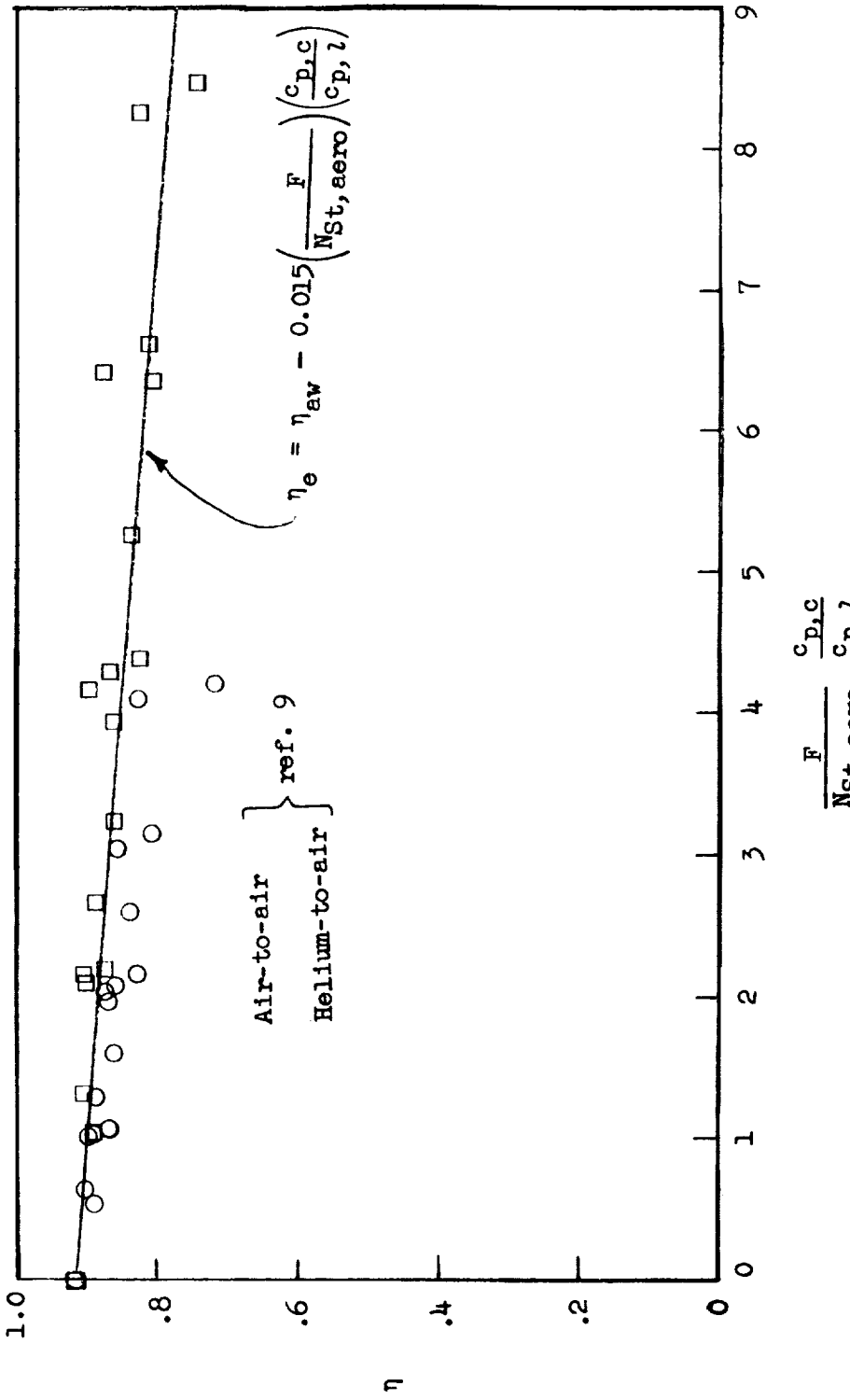

Figure 15.- Variation of boundary-layer recovery factor with the flow-rate correlation parameter.

NASA - Langley Field, Va. L-892